J. Am. Soc. Mass Spectrom. (2017) 28:539–550
DOI: 10.1007/s13361-016-1575-x

RESEARCH ARTICLE

Vibrational Signatures of Isomeric Lithiated N-acetyl-D-hexosamines by Gas-Phase Infrared Multiple-Photon Dissociation (IRMPD) Spectroscopy

Yanglan Tan,[1,2] Ning Zhao,[1] Jinfeng Liu,[3] Pengfei Li,[4] Corey N. Stedwell,[1] Long Yu,[1] Nicolas C. Polfer[1]

[1]Department of Chemistry, University of Florida, Gainesville, FL 32611, USA
[2]*Present Address:* Institute for Nutritional Sciences, Shanghai Institutes for Biological Sciences, Chinese Academy of Sciences, Shanghai, 200031, China
[3]State Key Laboratory of Precision Spectroscopy, Institute of Theoretical and Computational Science, East China Normal University, Shanghai, 200062, China
[4]Department of Chemistry, Michigan State University, East Lansing, MI 48824, USA

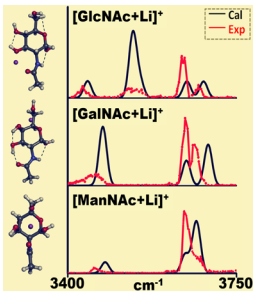

Abstract. Three lithiated N-acetyl-D-hexosamine (HexNAc) isomers, N-acetyl-D-glucosamine (GlcNAc), N-acetyl-D-galactosamine (GalNAc), and N-acetyl-D-mannosamine (ManNAc) are investigated as model monosaccharide derivatives by gas-phase infrared multiple-photon dissociation (IRMPD) spectroscopy. The hydrogen stretching region, which is attributed to OH and NH stretching modes, reveals some distinguishing spectral features of the lithium-adducted complexes that are useful in terms of differentiating these isomers. In order to understand the effect of lithium coordination on saccharide structure, and therefore anomericity, chair configuration, and hydrogen bonding networks, the conformational preferences of lithiated GlcNAc, GalNAc, and ManNAc are studied by comparing the experimental measurements with density functional theory (DFT) calculations. The experimental results of lithiated GlcNAc and GalNAc show a good match to the theoretical spectra of low-energy structures adopting a $^4C_1$ chair conformation, consistent with this motif being the dominant conformation in condensed-phase monosaccharides. The epimerization effect upon going to lithiated ManNAc is significant, as in this case the $^1C_4$ chair conformers give a more compelling match with the experimental results, consistent with their lower calculated energies. A contrasting computational study of these monosaccharides in their neutral form suggests that the lithium cation coordination with Lewis base oxygens can play a key role in favoring particular structural motifs (e.g., a $^4C_1$ versus $^1C_4$) and disrupting hydrogen bond networks, thus exhibiting specific IR spectral features between these closely related lithium-chelated complexes.

Keywords: Lithiated N-acetyl-D-hexosamine, IRMPD spectroscopy, Mass spectrometry, Vibrational signatures, Gas-phase conformations

Received: 17 August 2016/Revised: 22 November 2016/Accepted: 25 November 2016/Published Online: 3 January 2017

Introduction

Carbohydrates and their derivatives play key roles in numerous biological functions, such as cell growth, fertilization, and inflammation [1–4]. The vast number of carbohydrate variants, referred to as the isomer barrier [5], present a key challenge for their structural identification. While nuclear magnetic resonance (NMR) is generally considered the key technique in terms of identification [6–8], mass spectrometry (MS) has demonstrated an ability to gain important insights into their structures [9–18].

Monosaccharides are the smallest units and fundamental building blocks within the family of carbohydrates, representing a much smaller subset of isomeric variants that

Electronic supplementary material The online version of this article (doi:10.1007/s13361-016-1575-x) contains supplementary material, which is available to authorized users.

Correspondence to: Nicolas C. Polfer; *e-mail:* polfer@chem.ufl.edu

need to be differentiated, and hence posing a more surmountable analytical challenge. Drift tube and traveling wave ion mobility mass spectrometry (IM-MS) has been applied for resolving monosaccharide variants [19, 20]. Infrared multiple photon dissociation-mass spectrometry (IRMPD-MS) has been utilized for structural differentiation of methyl-glucopyranoside anomers and methyl-D-glycoside isomers by Eyler and co-workers [21–23], and on glucuronic iduronic acid by Cagmat et al. [24]. A key aspect in all of those studies is the use of metal cations as a charge carrier. Metal ions have the advantage of increasing ionization efficiencies of monosaccharide variants, as shown for Li^+ [21, 22], Na^+ [20, 25], NH_4^+ [26], Cu^{2+} [15], and Pb^{2+} [27]. Metal chelation also intimately affects the ligand structure and reactivity [28]. Lithiated saccharides have been prevalently used because small-size Li^+ is bound tightly and makes compact complexes, generating most abundant cross-ring fragmentation [16, 21, 29, 30], which establishes the value of Li^+-monosaccharide complexes in the positive-mode MS analysis for isomeric identification.

In addition, metal chelation also affects the structures that are formed, as the metal cations interact in strong electrostatic interactions with electron-rich groups or atoms. In carbohydrates, hydroxyl oxygens present a natural target for such complexation, but carbonyl, sulfate, or phosphate oxygens, if present, offer competing sites for binding. Depending on the isomeric form, the binding interactions may differ substantially, potentially leading to different collision cross-sections for various isomers, and hence a separation by ion mobility. Similarly, metal complexation can have a distinct effect in infrared spectroscopy by, for instance, perturbing hydrogen bonding interactions between various OH groups, and thus shifting the vibrational frequencies of those modes.

Another interesting but challenging topic on monosaccharide structures is investigating their conformational preferences from a fundamental point of view. Some common D-hexapyranoses and their derivatives, such as glucose, galactose, mannose, and glucuronic acid, have been explored experimentally in aqueous solution or crystals, proving that these molecules usually exist in the $^4C_1$ chair conformation with C-4 pointing up and C-1 pointing down [31–34]. Also, hydrogen bond networks with hydroxyl groups as both hydrogen donors and receptors have been observed, even forming long, cooperative chains [35, 36]. Despite convincing spectroscopic observation and quantitation for monosaccharide conformers in condensed phase, the understanding of their gas-phase structural forms remains ambiguous. Comprehensive theoretical calculations with density functional theory have been conducted by Momany and coworkers, involving full geometry optimization and energy calculations on variable conformations of both α- and β-isomeric D-hexapyranose [37–39]. However, only a limited number of experimental evidences have been given towards the conformational forms of monosaccharides and their derivatives in vacuo. Among gas-phase approaches, IR spectroscopy is likely best placed to address detailed structural questions. In addition to the studies mentioned above by Eyler and co-workers [22, 23], and Cagmat et al. [24], Simons and coworkers carried out IR spectroscopic experiments to examine the gas-phase conformation of neutral phenyl β-D-glucopyranoside and phenyl β-D-galactopyranoside [40–42]. Bendiak and co-workers showed direct evidence for the ring opening of deprotonated D-aldohexoses by IRMPD spectroscopy [43]. In regards to protonated monosaccharide ions, Compagnon and coworkers distinguished isobaric glucosamine 6-phosphate and glucosamine 6-sulfate and discussed their gas-phase conformations based on IRMPD results [44]. For most IR spectroscopic studies, density functional theory (DFT) computations have been primarily employed to rationalize the experimental results and assist the determination of conformational preferences.

In this work, the structures of three isomeric lithiated N-acetyl-D-hexosamine (HexNAc) as model monosaccharide derivatives have been studied by coupling mass spectrometry and gas-phase IRMPD spectroscopy in the frequency range mainly from 3400 cm^{-1} to 3750 cm^{-1}. Previous work has contributed to identify conformers of lithiated methyl N-acetyl-D-glucosamine and N-acetyl-D-galactosamine with IRMPD spectroscopy in the region between 900 cm^{-1} and 1800 cm^{-1} [22]. However, compared with the congested nature of delocalized C–O stretching and H bending vibrations, infrared spectroscopy in the hydrogen stretching region adopted in this study can resolve specific NH and OH vibrations and thus aid conformer identification for sugars [45].

Experimental

Sample Preparation

In this study, N-acetyl-D-glucosamine (GlcNAc), N-acetyl-D-galactosamine (GalNAc), and N-acetyl-D-mannosamine (ManNAc) were considered. Lithiated HexNAc samples were prepared at a concentration of 0.1 mM in MeOH-water (80:20) solutions with equimolar concentration of LiCl. All reagents were purchased from Sigma Aldrich (St. Louis, MO, USA) and used without further purification.

Mass Spectrometry and Infrared Multiple Photon Dissociation (IRMPD)

All experiments were carried out using a custom-built mass spectrometer coupled with a tunable, continuous-wave (cw) optical parametric oscillator/amplifier (OPO/A) (LINOS Photonics OS4000, Munich, Germany). This setup has already been described in previous studies [46, 47]. Lithiated HexNAc was ionized in a modified electrospray ionization (ESI) source (Analytica, Branford, CT, USA) equipped with an rf ion funnel. Ions of interest were mass-selected by a quadrupole mass filter (Ardara Technologies LP, Ardara, PA, USA), followed by trapping and OPO/A irradiation in a reduced-pressure (background pressure ~10^{-5} mbar) quadrupole ion trap. Helium gas was pulsed to assist trapping of ions, and then pumped away prior to irradiation. The cw OPO/A was pumped by a cw Nd/YAG laser (1064 nm, 2W), generating an idler and a signal

beam through nonlinear interactions and quasi-phase matching within a periodically poled lithium niobate (PPLN) optical crystal. The idler beam was focused onto the ion cloud with a lens through an aperture in the ring electrode (2.4 mm diameter). In order to determine the idler wavelength used for IR irradiation, the signal wavelength was determined with a wave meter (EXFO WA-1000). The combined power of the idler beam was measured by reflecting them off a mechanical shutter (UNIBLITZ VS25S2ZMO) into a power meter (Ophir 3A). The mechanical shutter also allowed control of the irradiation time. A time-of-flight drift (TOF) tube (Jordan TOF Products, Grass Valley, CA, USA) was employed for mass analysis of the remaining precursor and photofragment(s).

In order to obtain well-resolved vibrational bands in IRMPD spectra, the irradiation time used in this study was optimized as 250 ms in the wavenumber range from 3600 to 3750 cm^{-1}, and 1000 ms in the wavenumber range below 3600 cm^{-1}, due to weaker IRMPD yields in the latter region. In order to normalize for the different irradiation times, the IRMPD yield in the wavenumber below 3600 cm^{-1} was divided by a factor of 4. At each laser frequency, a set of 10 mass spectra were collected and averaged. Data were analyzed with aid of an in-house LabVIEW program. The IRMPD yield was calculated by the formula,

$$\text{IRMPD Yield} = -\ln\left(1-\frac{\sum \text{fragment intensities}}{\sum \text{fragment intensities} + \text{precursor intensity}}\right)$$

Here, ∑fragment intensities was the total intensity of fragments. The idler power ranged between 20 and 60 mW, so the IRMPD yield was further normalized linearly with this power. All IRMPD spectra shown here were obtained by plotting the normalized IRMPD yields (by power and irradiation time) versus wavenumber of irradiation.

Calculations

Initial α- and β-HexNAc structures were built in Gabedit [48] using a systematic approach. Neutral monosaccharide conformations (e.g., chair conformations $^4C_1$ or $^1C_4$) were considered based on evidence from literature; various rotamers resulting from rotations of the C-5–C-6 bond, such as gauche-gauche (*gg*) and trans-gauche (*tg*), were explored to maximize hydrogen bonding interactions. This also included the clockwise (*c*) or counterclockwise (*r*) orientation of the hydroxyl groups. Lithium cations were initially placed above the sugar ring with the distances of 2–3 Å from the closest atom on the ring, and rotating moieties to maximize hydrogen bonding interactions.

$^4C_1$ chair conformations of each HexNAc isomer were considered as the starting structures for the sugar ring, prior to metal attachment and geometry optimization, since D-hexopyranose monosaccharide residues in glycosaminoglycans (GAGs) typically adopt the $^4C_1$ conformation (Scheme 1) [34]. However, for ManNAc structures, due to acetamido axial substitution at C-2, which is expected to be more hindered than the corresponding equatorial substitution, the $^4C_1$ chair conformations may be disfavored. Thus, corresponding flipped $^1C_4$ chair structures, and also skew forms $^1S_5$ and $^5S_1$, were built and calculated. The geometry optimizations and spectral computation of structures were performed on lithiated HexNAc, as well as neutral molecules without lithium ion chelation, by using the B3LYP/6-31 g+(d,p) level of theory in the Gaussian 09 package [49]. The energies are reported here as zero-point-energy (ZPE)-corrected energies (at 0 K) without scaling, both in atomic units (i.e., Hartrees), and as relative energies (kJ/mol). For the computed IR spectra, a uniform scaling factor of 0.958 [24] and a Gaussian profile (full width-half maximum, FWHM = 10 cm^{-1}) were used to facilitate comparison with the experimental results.

Results and Discussion

IRMPD Spectra of [GlcNAc + Li]$^+$, [GalNAc + Li]$^+$, and [ManNAc + Li]$^+$

Figure 1 displays the experimental IRMPD spectra of [GlcNAc + Li]$^+$, [GalNAc + Li]$^+$, and [ManNAc + Li]$^+$, respectively, in the wavenumber range from 3400 cm^{-1} to 3750 cm^{-1}, where vibrational bands are generally attributed to OH and NH stretching modes. The vibrational patterns of these closely-related molecules do exhibit some notable differences, which is a useful feature in terms of their identification and differentiation. The peaks observed in the higher-frequency 3640–3680 cm^{-1} range are most likely assigned to the various alcohol OH stretching modes. The bands around 3430 cm^{-1} and 3460 cm^{-1} are probably due to NH stretching. The NH stretching band for [GalNAc + Li]$^+$ and [ManNAc + Li]$^+$ exhibit a considerable 30 cm^{-1} blue-shift compared with [GlcNAc + Li]$^+$. Also, this band is rather broad for [GalNAc + Li]$^+$, suggesting multiple, unresolved features. Another significant distinguishing feature in the spectra of [GlcNAc + Li]$^+$ is the broad IR band centered at 3540 cm^{-1}, whereas nearly no photodissociation takes place for [GalNAc + Li]$^+$ and [ManNAc + Li]$^+$ in this range. It is possible that these bands arise from red-shifted OH stretches, which, however, needs to be verified with computations.

Calculated Spectra and Conformer Analysis for [GlcNAc + Li]$^+$

In order to obtain a deeper insight into gas-phase structures and interpret experimental IRMPD spectra, theoretical calculations of lithiated HexNAc conformers were carried out. A complicating factor in this is that each isomer in principle exists as a mixture of two anomers, α and β, since the anomeric end is unblocked and results in possible interconversion between α and β in solution. The many rotamers and clockwise/counterclockwise hydroxyl group orientations further increase the complexity for sugar conformational investigation. A final question lies in identifying the most favorable interactions between lithium and Lewis base oxygens in these structures,

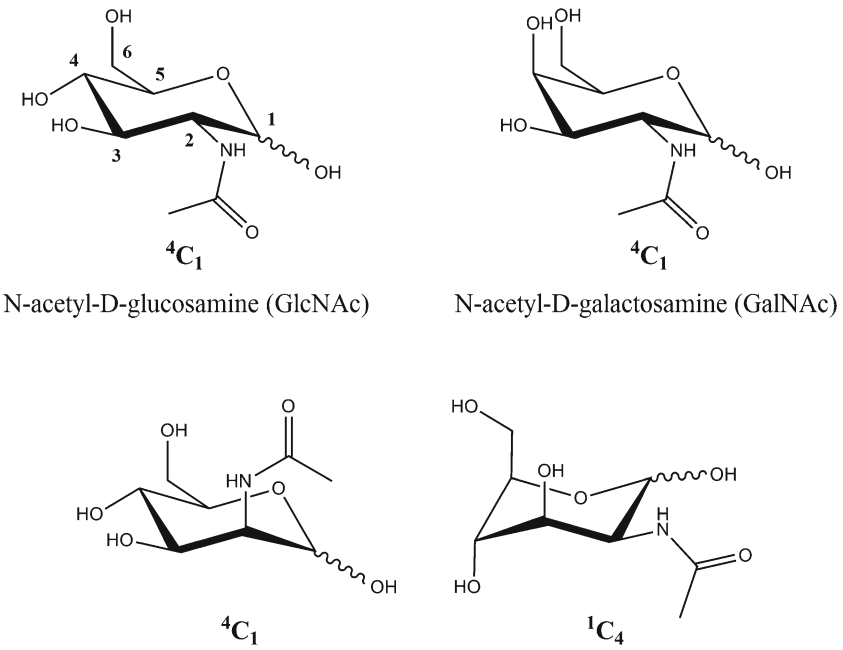

Scheme 1. Chair conformations considered in the theoretical calculations for lithiated and neutral GlcNAc, GalNAc, and ManNAc. Anomeric position is indicated by wiggly bond to denote presence of both α- and β-anomers. The numbering scheme for the carbon atoms is indicated for GlcNAc

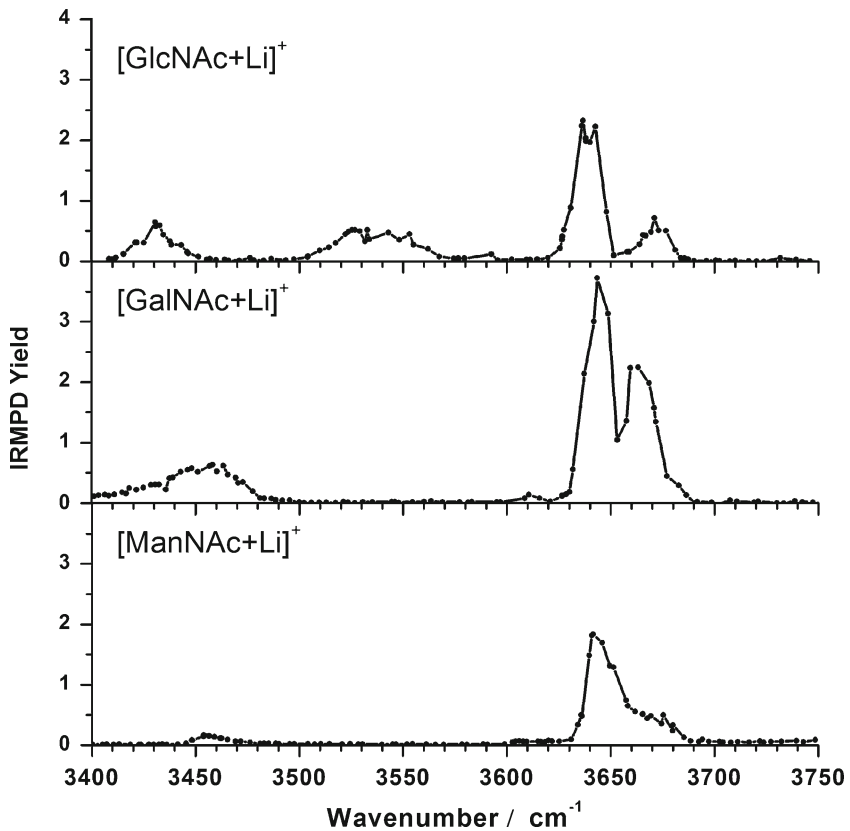

Figure 1. IRMPD spectra of lithiated GlcNAc, GalNAc, and ManNAc

Table 1. ZPE-Corrected Energies for Lithiated GlcNAc (structures presented in Figure 2, IRMPD spectrum of four low-energy conformers in shading shown in Figure 3)

	Structures	ZPE-corrected Energy (Hartree)	Relative Energy (kJ/mol)
A	Li^+(α-*gg*-$^4C_1$-c-GlcNAc)[CO,O3]	-827.194889	0
B	Li^+(β-*gg*-$^4C_1$-c-GlcNAc)[CO,O3]	-827.189284	14.7
C	Li^+(α-*gg*-$^4C_1$-c-GlcNAc)[CO,O1]	-827.176342	48.7
D	Li^+(β-*gg*-$^4C_1$-c-GlcNAc)[CO,O1]	-827.185907	23.6
E	Li^+(α-*tg*-$^4C_1$-c-GlcNAc)[CO,O3]	-827.159621	92.6
F	Li^+(β-*tg*-$^4C_1$-c-GlcNAc)[CO,O3]	-827.154080	107.1
G	Li^+(α-*tg*-$^4C_1$-c-GlcNAc)[CO,O1]	-827.144213	133.0
H	Li^+(β-*tg*-$^4C_1$-c-GlcNAc)[CO,O1]	-827.149862	118.2

to rationalize how metal chelation affects the structure and thus the vibrational features.

NMR results showed that *gg*-$^4C_1$ predominated in both α- and β-D-glucopyranose conformational populations in solution [50]. In vacuo DFT studies gave energies of D-glucopyranose rotamers in favor of the *gg*- and *tg*-$^4C_1$ conformation [37, 51]. For GlcNAc with the 2-acetamido substitution, Sattelle and Almond found a α-*gg*-$^4C_1$-r model as the most populated conformer in a 20 explicit solvent simulation [52]. Contreras et al. proposed and demonstrated a favored *tg*-$^4C_1$-c conformation in their study of anomerically locked methyl GlcNAc complexed to Li^+ by experimental IRMPD spectra in carbonyl stretching band positions. The calculated energies for optimized neutral *gg*-$^4C_1$(-c/-r) and *tg*-$^4C_1$-c GlcNAc in our study revealed an α-*gg*-$^4C_1$-r-GlcNAc structure as the most stable conformer (Supplementary Table S1, Supplementary Figure S1, Supporting Information), which is very analogous to the lowest-energy structure in Sattelle's solution-phase

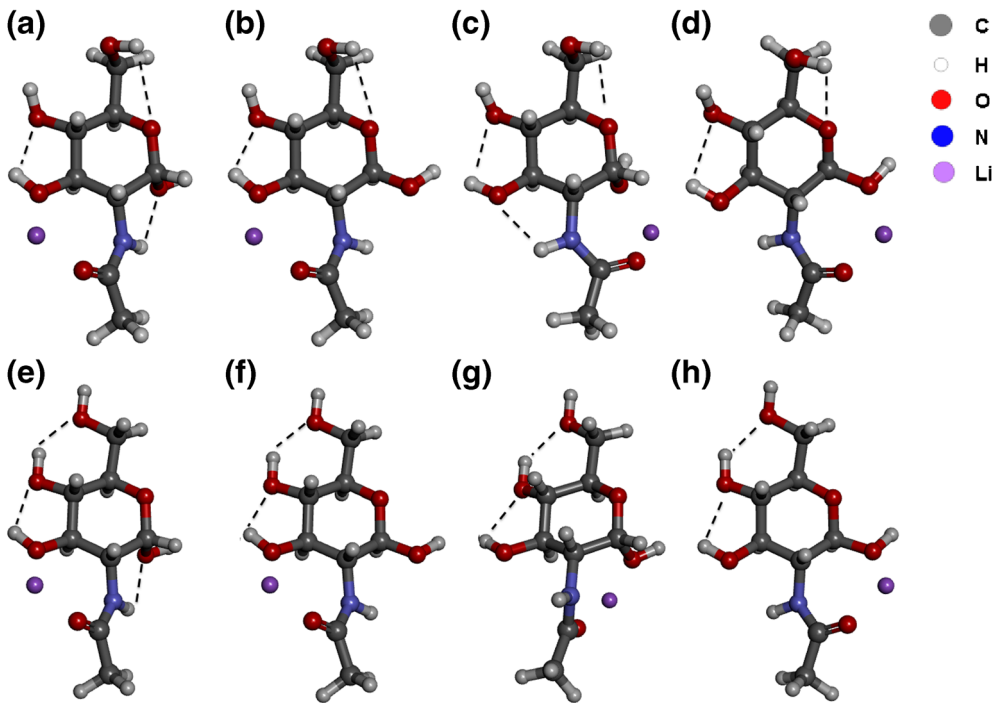

Figure 2. Geometry-optimized $^4C_1$ chair conformers of lithiated α-/β-GlcNAc generated from DFT calculations, with hydrogen bonds shown as dashed lines. More detail on these structures is given in Table 1

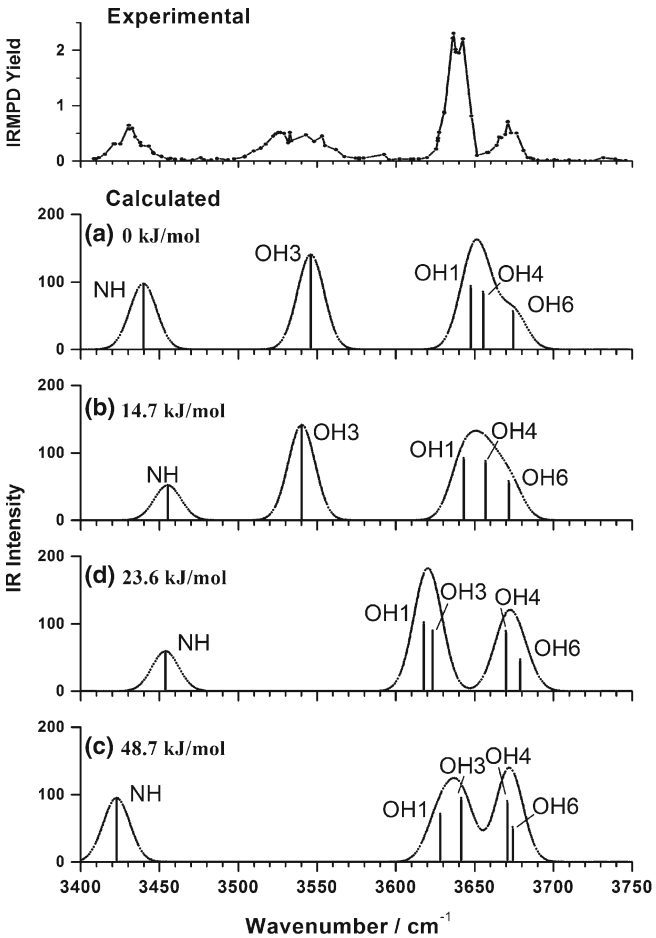

Figure 3. Comparison of experimental IRMPD spectrum with calculated infrared spectra for four lowest-energy $^4C_1$ chair conformers of lithiated GlcNAc shown in Figure 2

computation [52]. Therefore, the theoretical investigation in the structural preference of lithiated GlcNAc mainly focused on *gg*-$^4C_1$ and *tg*-$^4C_1$ rotamers complexed to Li^+ here.

The calculated geometry-optimized *gg*-$^4C_1$ and *tg*-$^4C_1$ structures of lithiated α-/β-GlcNAc are presented in Table 1 and Figure 2. For the sake of simplicity, the structures are referred to as structures A–H, to denote the Figure in which they appear. The numbering system for the OH groups follows the same numbering system as the corresponding carbon on the pyranose ring; in other words, OH-3 denotes the hydroxyl group bound to C-3. Here, we also specify each oxygen interacting with Li^+ using the nomenclature adopted by Heaton and Armentrout et al. [53], where [CO,O3] for instance denotes the coordination of lithium ion with both the oxygen of the carbonyl group and oxygen of the OH-3 group. The calculated lowest-energy structure of lithiated GlcNAc (structure A) adopts the α-*gg*-$^4C_1$-c motif in which the lithium ion interacts with both the oxygen of the carbonyl group and oxygen of the OH-3 group. Although the counterclockwise orientation of hydrogen bonds in neutral GlcNAc was preferred as mentioned above, the lithium ion interaction causes the change in the orientation of hydrogen bonds in the lowest-energy Li^+[CO,O3] model. The minimum-energy *tg*-$^4C_1$ conformers (structure E and F) with a cooperative OH-3…OH-4…OH-6 hydrogen bonding possess similar Li^+ coordination as well. In an alternative binding pattern investigated here, Li^+ interacts with the carbonyl oxygen and the oxygen of OH-1 for both *gg*- (structure C and D) and *tg*- (structure G and H) rotamers. More detail on these structures is given in Table 1, such as the ZPE-corrected energies in atomic units (i.e., Hartrees), as well as their chair configurations and anomericities.

The experimental IRMPD spectra of lithiated GlcNAc and the calculated infrared spectra for the four lowest-energy structures, shown in shading in Table 1, are presented in Figure 3 with their relative energies indicated. The four structures are all in the *gg*-$^4C_1$ conformation with both α- and β-anomericity and different lithium ion binding patterns, which implies that *gg*-conformation was more stable for lithiated GlcNAc than *tg*-conformation by ~90 kJ/mol. In Figure 3, the annotation of the vibrations follows the same scheme as for the OH groups, but in order to distinguish between chemical moieties and vibrations, groups are hyphenated (e.g., OH-2), whereas vibrations (e.g., OH2) are not. The computational results suggest that for lithiated GlcNAc, the anomeric configuration has little effect on the IR absorption spectra, but that the interaction patterns between the lithium ion and sugar molecule result in significant shifts in IR spectra. A comparison of the experimental IRMPD

Table 2. ZPE-Corrected Energies for Lithiated GalNAc (structures presented in Figure 4, IRMPD spectrum of four low-energy conformers in shading shown in Figure 5)

	Structures	ZPE-corrected Energy (Hartree)	Relative Energy (kJ/mol)
A	Li^+(α-*gg*-$^4C_1$-c-GalNAc)[CO,O3,O4]	-827.202268	0
B	Li^+(β-*gg*-$^4C_1$-c-GalNAc)[CO,O3,O4]	-827.194169	21.3
C	Li^+(α-*gg*-$^4C_1$-r-GalNAc)[O4,O5,O6]	-827.192189	26.5
D	Li^+(β-*gg*-$^4C_1$-r-GalNAc)[O4,O5,O6]	-827.186159	42.3
E	Li^+(α-*tg*-$^4C_1$-c-GlcNAc)[CO,O3,O4]	-827.159045	113.5
F	Li^+(β-*tg*-$^4C_1$-c-GlcNAc)[CO,O3,O4]	-827.151588	133.1

spectrum for $[GlcNAc + Li]^+$ shows that conformers A and B, other than C and D, can account for the bands that are observed experimentally. The calculation results indicate that the characteristic IR band at 3540 cm^{-1} is explained by the stretching modes OH3 that are red-shifted remarkably by lithium ion interaction. The minor differences between the computed spectra for structures A and B do not provide sufficient evidence to discriminate between both anomers, or determine their relative contributions in the gas phase.

Calculated Spectra and Conformer Analysis for $[GalNAc + Li]^+$

GalNAc is the C-4 hydroxyl epimer of GlcNAc. ^{1}HNMR [32, 54, 55] and X-ray crystallography [32, 56–58] analysis of galactose and its derivative demonstrated $^4C_1$ chair as the dominant conformation in galactose analogs. β-Anomericity of galactose was reported to be strongly favored in solution [59], whereas the α-anomer was preferred by previous in vacuo DFT results [37, 38]. Momany et al. reported that the α-*gg*-$^4C_1$-c conformation was the lowest-energy glucopyranose structure from a DFT study. Our computational results of neutral *gg*-GalNAc showed that an α-*gg*-$^4C_1$-r conformer with the counterclockwise hydrogen-bonding orientation was energetically preferred (Supplementary Table S2, Supplementary Figure S2). For lithium–methyl GalNAc complexes, IRMPD spectra in the range 900–1800 cm^{-1} provided the evidence for the predominant *gg*-$^4C_1$-r conformation. By referring to these experimental and theoretical results, conformational preferences of lithium-GalNAc adducts were explored based on *gg*-$^4C_1$ and *tg*-$^4C_1$ models in this study. The structures and energy of the geometry-optimized conformers are shown in Table 2 and Figure 4.

The calculated minimum-energy conformer for lithiated GalNAc is shown as structure A in Figure 4, with the α-*gg* conformation and a tridentate interaction between Li^+ and electron lone pairs of O-3, O-5, and oxygen at acetamido group. It exhibits three intramolecular hydrogen bonds between OH-4 and OH-6, OH-6, and O-5, and the glycosidic oxygen and amide hydrogen. The calculated structure B for lithiated β-GalNAc, which is second-lowest in energy, has a similar Li^+–oxygen tridentate interaction as well, but contains only two hydrogen bonds between OH-4 and OH-6, and OH-6 and O-5. As shown in Figure 4, after geometry optimization of [GalNAc

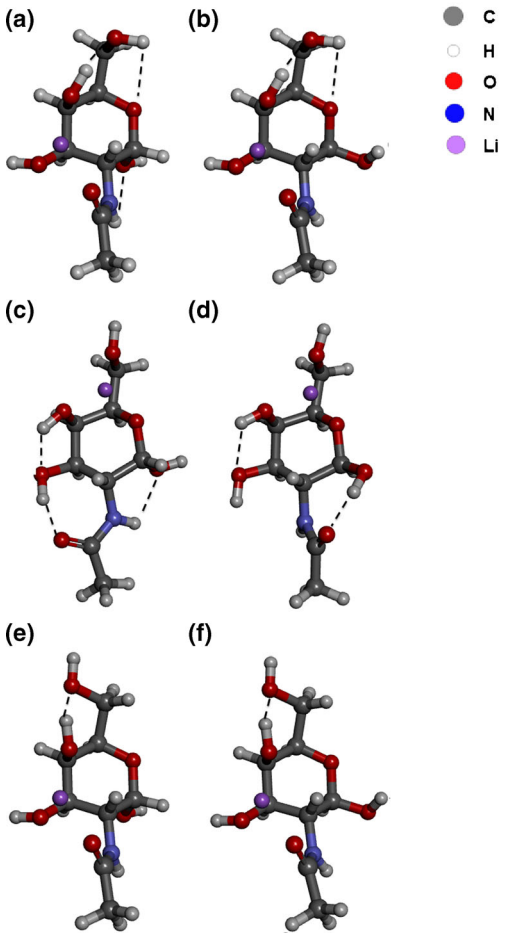

Figure 4. Geometry-optimized $^4C_1$ chair conformers of lithiated α-/β-GalNAc generated from DFT calculations, with hydrogen bonds shown as dashed lines. More detail on these structures is given in Table 2

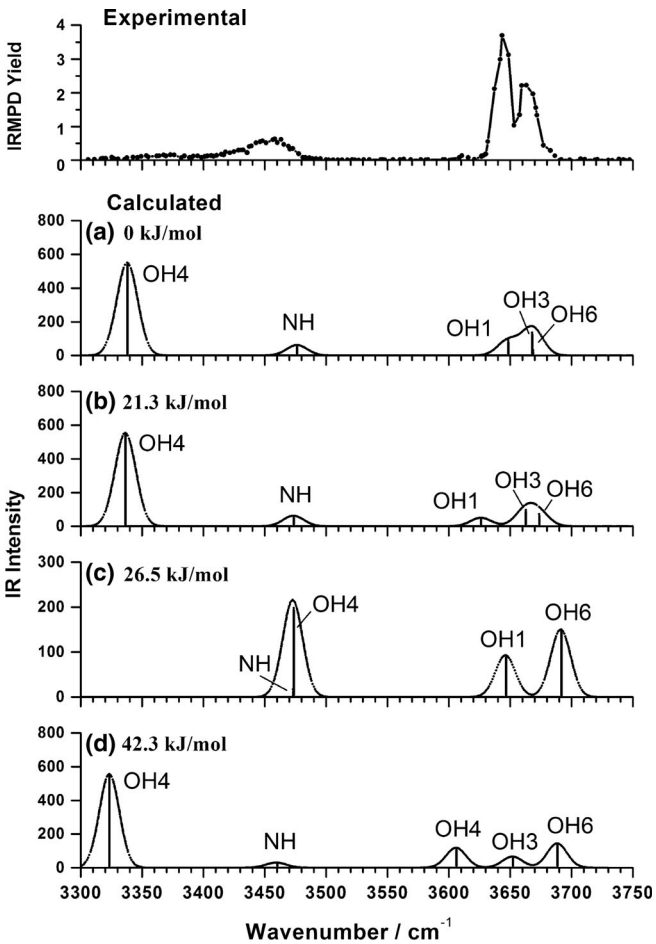

Figure 5. Comparison of experimental IRMPD spectrum with calculated infrared spectra for four lowest-energy $^4C_1$ chair conformers of lithiated GalNAc shown in Figure 4

Table 3. ZPE-Corrected Energies for Lithiated ManAc (structures presented in Figure 6, IRMPD spectrum of four low-energy conformers in shading shown in Figure 7)

	Structures	ZPE-corrected Energy (Hartree)	Relative Energy (kJ/mol)
A	Li^+(α-*tg*-$^4C_1$-c-ManNAc)[CO,O3]	-827.141362	134.8
B	Li^+(β-*tg*-$^4C_1$-c-ManNAc)[CO,O3]	-827.140600	136.8
C	Li^+(α-*gg*-$^1C_4$-c-ManNAc)[CO,O1]	-827.188660	10.6
D	Li^+(α-*gg*-$^1C_4$-c-ManNAc)[CO,O3]	-827.181517	29.3
E	Li^+(β-*gg*-$^1C_4$-c-ManNAc)[CO,O1,O3]	-827.191964	1.9
F	Li^+(α-*gg*-$^1C_4$-r-ManNAc)[CO,O1]	-827.181595	29.1
G	Li^+(β-*gg*-$^1C_4$-ManNAc)[CO,O1,O3,O6]	-827.192689	0
H	Li^+(β-*gg*-$^1S_5$-r-ManNAc)[CO,O1,O3]	-827.186680	15.8
I	Li^+(α-*gg*-$^5S_1$-r-ManNAc)[O1,O4,O5]	-827.168375	63.8

+ Li]$^+$ motifs, Li^+ exhibits a tridentate interaction with three oxygen atoms due to the axial position of OH-4.

As mentioned before, our particular interest in the experimental IRMPD spectrum of [GalNAc + Li]$^+$ is the broad and unresolved band, which is not typically attributed to a single NH stretching mode. The comparison of the experiment and theoretical spectra of four lowest-energy conformers shown in shading in Table 2 is presented in Figure 5, indicating a best match between the experimental result and calculated structure C, which is Li^+(α-*gg*-$^4C_1$-r-GalNAc)[O4, O5, O6] and very analogous to that found by Contreras et al. in their study of anomerically locked methyl-D-GalNAc complexed to Li^+ [22]. As expected, the peaks observed at 3640 cm^{-1} and 3670 cm^{-1} are assigned to OH stretching, namely OH1 and OH6, even if the latter peak shows a 30 cm^{-1} red shift compared with the calculated OH-6 stretching band. The broad band between

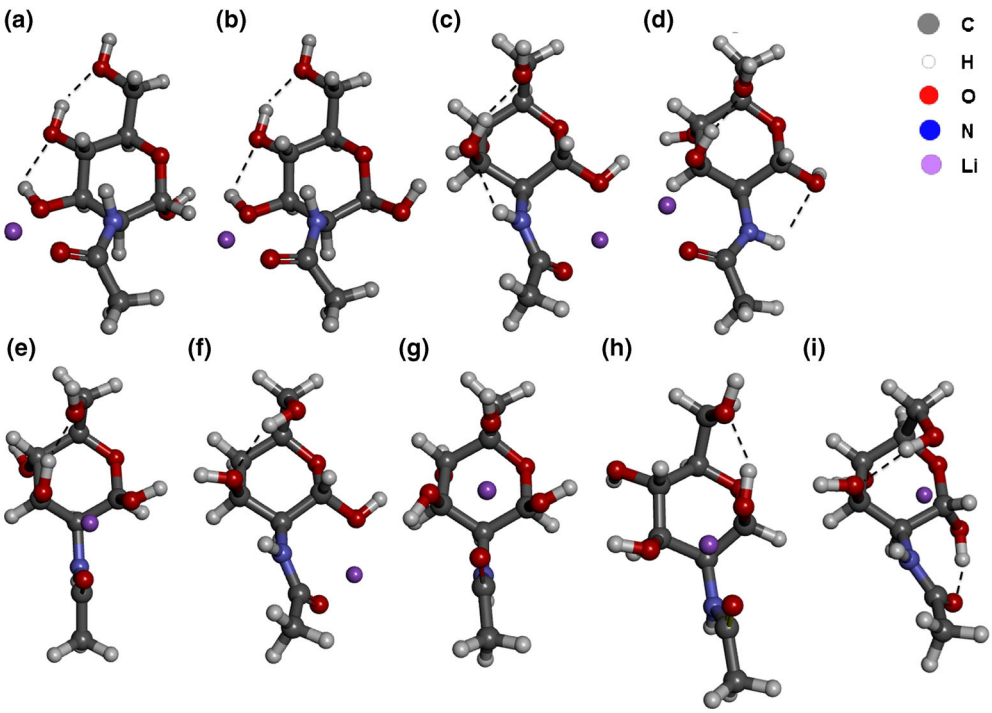

Figure 6. Geometry-optimized $^4C_1$ chair, $^1C_4$ chair, $^1S_5$ skew, and $^5S_1$ skew conformers of lithiated α-/β-ManNAc generated from DFT calculations, with hydrogen bonds shown as dashed lines. More detail on these structures is given in Table 3

3400 cm^{-1} and 3500 cm^{-1} is attributed to two unresolved modes of NH and OH4. By comparing with structure C with α-anomericity, the β-anomer structure D possesses a different hydrogen bonding pattern and thus shows distinguishing vibrational features. The spectra of the two lowest-energy conformers, structure A and B, appear to be different with the strong OH4 feature not seen in the experiment. Despite being energetically favorable, these two conformers are not supported by the experiment, and are probably absent or only present in trace amounts in the gas phase. Interestingly, the best-matched IR spectrum for Li^+(α-*gg*-$^4C_1$-r-GalNAc)[O4,O5,O6] (structure C) also correlates with the lowest-energy structure of the neutral α-*gg*-$^4C_1$-r-GalNAc form (structure C in Supplementary Table S2, Supplementary Figure S2). These results suggest that the global minimum structure may not always be accessible for metal-chelated sugars, and that the energetics of the neutral forms can play a role in which metal-chelation pattern is preferentially adopted.

Calculated Spectra and Conformer Analysis for [ManNAc + Li]$^+$

ManNAc is the C-2 acetamido-substituted epimer of GlcNAc. Some previous studies of mannopyranose have shown that the hydroxyl epimerization at the C-2 position does not change the $^4C_1$ chair conformation, for example in the crystal environment and solution [33, 60]. Appell et al. gave an energy sequence of mannopyranose conformation $^4C_1$ chair < $^1C_4$ chair < skew forms < boat forms in a general observation by DFT computations [39]. Specifically, *tg* was favored in both α- and β-mannopyranose with $^4C_1$ chair conformation and *gg* was preferred among $^1C_4$ conformers. With regard to ManNAc, the configuration at the C-2 position places the acetamido group in the axial position in the $^4C_1$ pyranose ring, which brings about much more steric hindrance compared with an axial hydroxyl group. Our calculation results of neutral *tg*-$^4C_1$-ManNAc and *gg*-$^1C_4$-ManNAc (Supplementary Table S3, Supplementary Figure S3) showed that $^4C_1$ was still the preferred conformation despite of the C-2 epimerization effects.

So far, few investigations have been conducted towards the conformational preference of mannose analogs complexed to metal cations. For theoretical calculations of lithiated ManNAc, the *tg*-$^4C_1$ and *gg*-$^1C_4$ conformation, which exchange the positions of the axial and equatorial substituents, were studied here. Because the interaction between lithium ion and oxygen atoms of more axial hydroxyl groups, particularly in "flipped" $^1C_4$ chair conformations, may be energetically favored, more putative structures with various lithium binding motif and hydrogen bonding orientation were calculated. Beside chair conformations, lithium-adducted *gg*-$^1S_5$-ManNAc and *gg*-$^5S_1$-ManNAc were also considered, since they were theoretically the most stable skew forms of in vacuo mannopyranose [39]. These geometry-optimized conformers of lithiated ManNAc are shown in Table 3 and Figure 6.

Two minimum-energy structures, G and E, adopt the β-*gg*-$^1C_4$ conformation with different lithium coordination towards four and three oxygen atoms, respectively. Structure G is the most favored energetically because it is stabilized by a tetradentate interaction between Li^+ and oxygen atoms at acetamido, OH-1, OH-3, and OH-6, with 1.9–2.0 Å distance between Li^+ and each oxygen atom. The enhanced chelation of the metal cation via a larger coordination number results in a lower energy, despite the fact that putative hydrogen bonding interactions are disrupted. Similar with structure E, structure H exhibits the tridentate interaction between Li^+ and O-3, O-5 and the oxygen at the acetamido group, but the non-identical distance between parallel axial hydroxyl groups in chair and skew forms leads to different hydrogen bonds in their structures. Structure C is the lowest-energy conformer with coordination number of two, where lithium ion interacts with oxygen at acetamido and OH-1, and a NH…OH-3…OH-6 hydrogen boding chain is observed, since the parallel axial configuration of OH-3 and the 5-

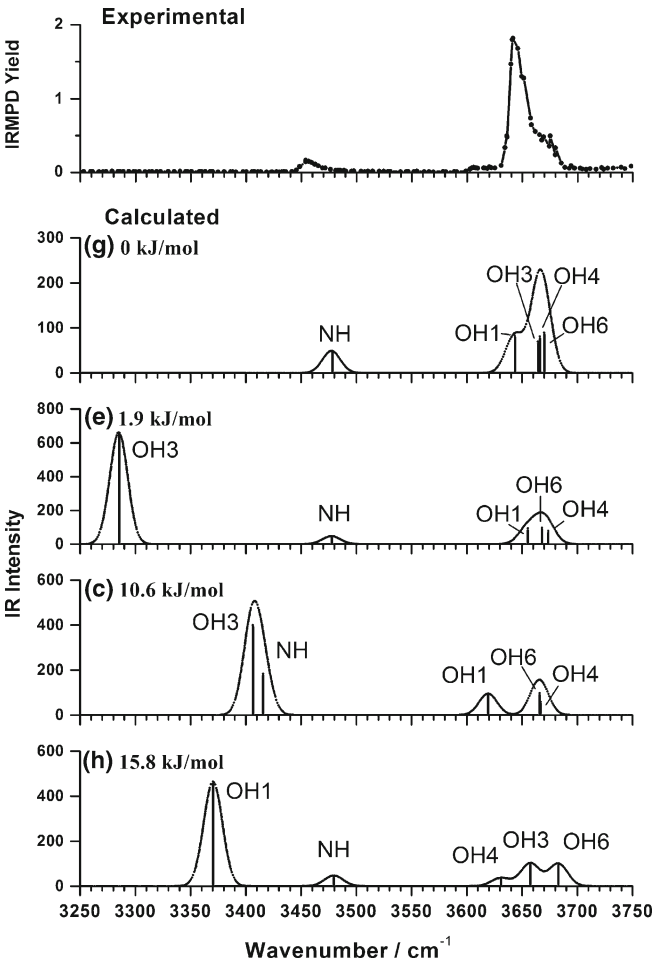

Figure 7. Comparison of experimental IRMPD spectrum and calculated infrared spectra for four low-energy conformers ($^1C_4$ chair and $^1S_5$ skew included) of lithiated ManNAc with structures shown in Figure 6

hydroxylmethyl group decreases the distance between OH-3 and OH-6.

Consistent with energy calculation results, the theoretical IR spectra of structure G shows the best match to the experimental spectra of lithiated ManNAc (Figure 7). Conversely, other low-energy structure E, C, and H all predict modes that are not confirmed experimentally. The broad peak at 3630–3690 cm^{-1} is assigned to coupled OH-1, OH-3, OH-4, and OH-6 stretching modes. The low-intensity, resolved band at 3460 cm^{-1} corresponds to the NH stretching mode and shows a 20 cm^{-1} red shift compared with the calculated result. In summary, the comparison with theory suggests that the β-$^{1}C_{4}$ conformation with a tetradentate Li^{+} coordination is predominantly observed in the gas phase.

Theoretical Calculations of Neutral GlcNAc, GalNAc, and ManNAc

In order to study the influence of lithium ion chelation on the preferred conformations and IR spectra of these saccharides in more detail, theoretical computions of neutral GlcNAc, GalNAc, and ManNAc molecules were compared with the lithiated results. Unfortunately, the experimental spectra of these neutral monosaccharides acquired in the condensed phase have poor resolution in the hydrogen stretching region [61] due to solvent absorption and strong intermolecular interactions (e.g., hydrogen bonds), and are hence of limited use here. Note that IR spectra in the far-IR (i.e., THz) range are highly informative in terms molecular identification [62]. The corresponding α-/β-GlcNAc and α-/β-GalNAc with $^{4}C_{1}$ chair conformation, and α-/β-ManNAc with both $^{4}C_{1}$ and $^{1}C_{4}$ chair conformations, were considered and shown in Supplementary Figures S1–S3, and their corresponding energies shown in Supplementary Tables S1–S3.

There are some general observations that can be made when comparing the computations for the neutral and lithiated forms. Lithium ion chelation causes significant energy differences between α- and β-anomers, whereas in the neutral form α- and β- are much closer in energy. More elaborate hydrogen bonding networks are formed within HexNAc molecules without lithium ion interaction.

For ManNAc, the C-2 epimer of GlcNAc is remarkably sensitive to lithium ion internal coordination in terms of energy and thus conformational preference. For the neutral form, the $^{4}C_{1}$ chair conformation is favored over the $^{1}C_{4}$ conformation. The reverse is true in the lithiated case, implying that the chelation effect upon ManNAc by lithium ion is the dominant determinant for the structural preference.

Fragmentation Patterns

The IRMPD spectra exhibit vibrational features that in principle allow a differentiation between these three lithium-adducted isomers. Representative mass spectra

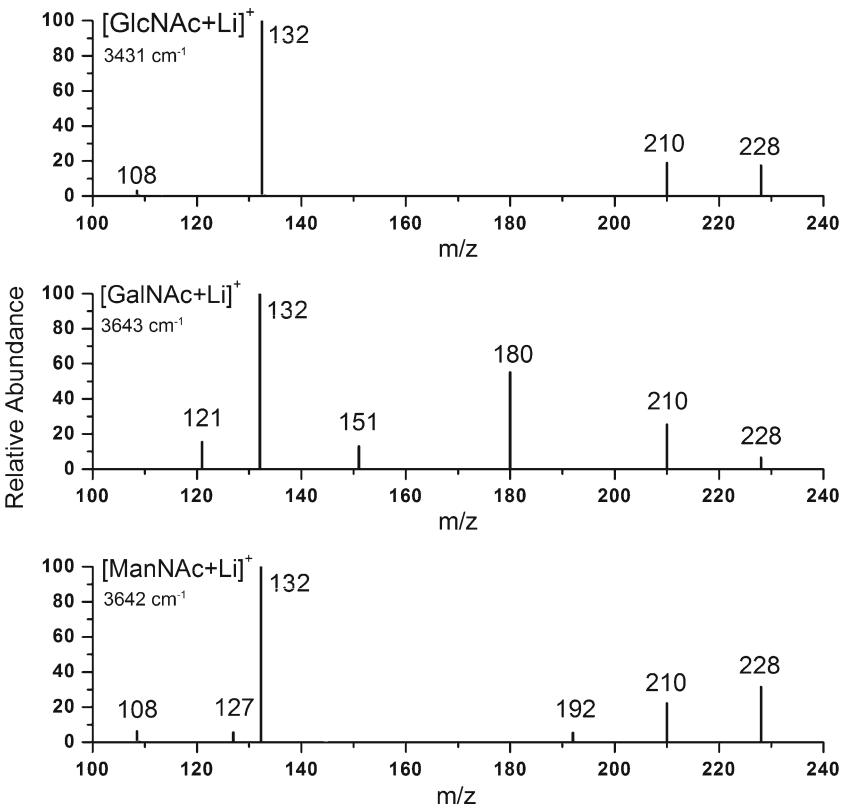

Figure 8. IRMPD mass spectra of lithiated GlcNAc, GalNAc, and ManNAc with IR irradiation at the corresponding wavenumber where maximum fragmentation was obtained

of these three lithiated N-aceytlhexosamines at the corresponding wave number of maximum IRMPD yields are shown in Figure 8. The dissociation patterns of lithiated HexNAc indicate the presence of some diagnostic product ions, as summarized in Supplementary Table S4, such as *m/z* 121,151, and 180 for $[GlcNAc + Li]^+$ and *m/z* 127 and 192 for $[ManNAc + Li]^+$. The combination of characteristic IR absorbances and photodissociation products illustrate the selective information on isomers that can be obtained with these measurements.

As a comparison, lithiated ManNAc was also dissociated via collision-induced dissociation (CID), as shown in Supplementary Figure S4. Similar fragment types were produced in both IRMPD and CID spectra, except for the prominent absence of the *m/z* 150 CID product. As the appearance of fragmentation products is dependent on the activation energy and timescale, and these parameters are different for IRMPD and CID, it is not surprising to see some differences in the results. Another important difference in IRMPD vis-à-vis CID is the fact that in IRMPD photofragment products may absorb subsequent photons at a resonant frequency, and may hence be subject to sequential fragmentation. It is likely that the *m/z* 150 product strongly absorbs photons at 3642 cm^{-1}, and is hence not observed in the IRMPD mass spectrum.

Conclusions

The monosaccharide epimers GlcNAc, GalNAc, and ManNAc were complexed with lithium and studied via IRMPD spectroscopy in the hydrogen stretching region. A structural interpretation of these results was based on DFT computations, yielding the following conclusions. There are differences in the IRMPD spectra and photodissociation product ions between the various monosaccharide epimers; the selective information on each isomer is useful in terms of differentiating these molecules by mass spectrometry. The comparison between experimental IRMPD spectra and calculated results of low-energy conformations can rationalize the experimental band positions, thus allowing investigation of conformational preferences of gas-phase lithium-monosaccharides, as well as an interpretation of the role of metal ion chelation on structure and the observed IR spectrum. Whereas the $^4C_1$ chair conformation is favored for lithiated GlcNAc and GalNAc, the $^1C_4$ structure is favored for ManNAc; a tetradentate interaction of lithium with oxygen atoms at acetamido and hydroxyl groups is found to be responsible for stabilizing the $^1C_4$ chair conformation.

Acknowledgment

The project was financially supported by the United States National Science Foundation (NSF) under grant number CHE-1403262.

References

1. Varki, A.: Biological roles of oligosaccharides: all of the theories are correct. Glycobiology **3**, 97–130 (1993)
2. Dwek, R.A.: Glycobiology: toward understanding the function of sugars. Chem. Rev. **96**, 683–720 (1996)
3. Taylor, M.E., Drickamer, K.: Introduction to glycobiology, pp. 123–239. Oxford University Press, Oxford, UK (2003)
4. Fu, L., Suflita, M., Linhardt, R.J.: Bioengineered heparins and heparan sulfates. Adv. Drug Deliv. Rev. **97**, 237–249 (2016)
5. Laine, R.A.: A calculation of all possible oligosaccharide isomers both branched and linear yields 1.05×10^{12} structures for a reducing hexasaccharide: the isomer barrier to development of single-method saccharide sequencing or synthesis systems. Glycobiology **4**, 759–767 (1994)
6. Armstrong, G.S., Bendiak, B.: High-resolution four-dimensional carbon-correlate H-1-H-1 ROESY experiments employing isotags and the filter diagonalization method for effective assignment of glycosidic linkages in oligosaccharides. J. Magn. Reson. **181**, 79–88 (2006)
7. Bendiak, B., Fang, T.T., Jones, D.N.M.: An effective strategy for structural elucidation of oligosaccharides through NMR spectroscopy combined with peracetylation using doubly ^{13}C-labeled acetyl groups. Can. J. Chem. **80**, 1032–1050 (2002)
8. Bush, C.A., Martin-Pastor, M., Imberty, A.: Structure and conformation of complex carbohydrates of glycoproteins, glycolipids, and bacterial polysaccharides. Annu. Rev. Biophys. Biomol. Struct. **28**, 269–293 (1999)
9. Konda, C., Bendiak, B., Xia, Y.: Linkage determination of linear oligosaccharides by MS^n ($n > 2$) Collision-induced dissociation of Z_1 ions in the negative ion mode. J. Am. Soc. Mass Spectrom. **25**, 248–257 (2014)
10. Tan, Y.L., Polfer, N.C.: Linkage and anomeric differentiation in trisaccharides by sequential fragmentation and variable-wavelength infrared photodissociation. J. Am. Soc. Mass Spectrom. **26**, 359–368 (2015)
11. Fu, L., Li, G.Y., Yang, B., Onishi, A., Li, L.Y., Sun, P.L., Zhang, F.M., Linhardt, R.J.: Structural characterization of pharmaceutical heparins prepared from different animal tissues. J. Pharm. Sci. **102**, 1447–1457 (2013)
12. Lancaster, K.S., An, H.J., Li, B.S., Lebrilla, C.B.: Interrogation of N-linked oligosaccharides using infrared multiphoton dissociation in FT-ICR mass spectrometry. Anal. Chem. **78**, 4990–4997 (2006)
13. Devakumar, A., Thompson, M.S., Reilly, J.P.: Fragmentation of oligosaccharide ions with 157 nm vacuum ultraviolet light. Rapid Commun. Mass Spectrom. **19**, 2313–2320 (2005)
14. Li, G.Y., Cai, C., Li, L.Y., Fu, L., Chang, Y.Q., Zhang, F.M., Toida, T., Xue, C.H., Linhardt, R.J.: Method to detect contaminants in heparin using radical depolymerization and liquid chromatography-mass spectrometry. Anal. Chem. **86**, 326–330 (2014)
15. Desaire, H., Leary, J.A.: Differentiation of diastereomeric N-acetylhexosamine monosaccharides using ion trap tandem mass spectrometry. Anal. Chem. **71**, 1997–2002 (1999)
16. Polfer, N.C., Valle, J.J., Moore, D.T., Oomens, J., Eyler, J.R., Bendiak, B.: Differentiation of isomers by wavelength-tunable infrared multiple-photon dissociation-mass spectrometry: Application to glucose-containing disaccharides. Anal. Chem. **78**, 670–679 (2006)
17. Ashline, D.J., Hanneman, A.J.S., Zhang, H.L., Reinhold, V.N.: Structural documentation of glycan epitopes: sequential mass spectrometry and spectral matching. J. Am. Soc. Mass Spectrom. **25**, 444–453 (2014)
18. Kailemia, M.J., Li, L.Y., Xu, Y.M., Liu, J., Linhardt, R.J., Amster, I.J.: Structurally informative tandem mass spectrometry of highly sulfated natural and chemoenzymatically synthesized heparin and heparan sulfate glycosaminoglycans. Mol. Cell. Proteom. **12**, 979–990 (2013)
19. Gaye, M.M., Nagy, G., Clemmer, D.E., Pohl, N.L.B.: Multidimensional analysis of 16 glucose isomers by ion mobility spectrometry. Anal. Chem. **88**, 2335–2344 (2016)
20. Li, H., Giles, K., Bendiak, B., Kaplan, K., Siems, W.F., Hill Jr., H.H.: Resolving structural isomers of monosaccharide methyl glycosides using drift tube and traveling wave ion mobility mass spectrometry. Anal. Chem. **84**, 3231–3239 (2012)
21. Stefan, S.E., Eyler, J.R.: Differentiation of methyl-glucopyranoside anomers by infrared multiple photon dissociation with a tunable CO_2 laser. Anal. Chem. **81**, 1224–1227 (2009)
22. Contreras, C.S., Polfer, N.C., Oomens, J., Steill, J.D., Bendiak, B., Eyler, J.R.: On the path to glycan conformer identification: gas-phase study of

the anomers of methyl glycosides of N-acetyl-D-glucosamine and N-acetyl-D-galactosamine. Int. J. Mass Spectrom. **330**, 285–294 (2012)
23. Pearson, W.L., Contreras, C.C., Powell, D., Berden, G., Oomens, J., Bendiak, B., Eyler, J.R.: Differentiation of rubidiated methyl-D-glycoside stereoisomers by infrared multiple-photon dissociation spectroscopy in the O–H and C–H stretching regions. J. Phys. Chem. B **119**, 12970–12981 (2015)
24. Cagmat, E.B., Szczepanski, J., Pearson, W.L., Powell, D.H., Eyler, J.R., Polfer, N.C.: Vibrational signatures of metal-chelated monosaccharide epimers: gas-phase infrared spectroscopy of Rb^+-tagged glucuronic and iduronic acid. Phys. Chem. Chem. Phys. **12**, 3474–3479 (2010)
25. Xia, B., Zhou, Y., Liu, X., Xiao, J., Liu, Q., Gu, Y.C., Ding, L.S.: Use of electrospray ionization ion-trap tandem mass spectrometry and principal component analysis to directly distinguish monosaccharides. Rapid Commun. Mass Spectrom. **26**, 1259–1264 (2012)
26. Madhusudanan, K.P.: Tandem mass spectra of ammonium adducts of monosaccharides: Differentiation of diastereomers. J. Mass Spectrom. **41**, 1096–1104 (2006)
27. Salpin, J.Y., Tortajada, J.: Gas-phase reactivity of lead(II) ions with D-glucose. Combined electrospray ionization mass spectrometry and theoretical study. J. Phys. Chem. A **107**, 2943–2953 (2003)
28. Rodgers, M.T., Armentrout, P.B.: Cationic noncovalent interactions: energetics and periodic trends. Chem. Rev. **116**, 5642–5687 (2016)
29. Cancilla, M.T., Penn, S.G., Carroll, J.A., Lebrilla, C.B.: Coordination of alkali metals to oligosaccharides dictates fragmentation behavior in matrix assisted laser desorption ionization Fourier transform mass spectrometry. J. Am. Chem. Soc. **118**, 6736–6745 (1996)
30. Zhou, Z.R., Ogden, S., Leary, J.A.: Linkage position determination in oligosaccharides— mass spectrometry (MS/MS) study of lithium-cationized carbohydrates. J. Org. Chem. **55**, 5444–5446 (1990)
31. Maple, S.R., Allerhand, A.: Detailed tautomeric equilibrium of aqueous D-glucose. Observation of six tautomers by ultrahigh resolution carbon-13 NMR. J. Am. Chem. Soc. **109**, 3168–3169 (1987)
32. Roslund, M.U., Klika, K.D., Lehtila, R.L., Tahtinen, P., Sillanpaa, R., Leino, R.: Conformation of the galactose ring adopted in solution and in crystalline form as determined by experimental and DFT H-1 NMR and single-crystal X-ray analysis. J. Org. Chem. **69**, 18–25 (2004)
33. Angyal, S.J.: The composition and conformation of sugars in solution. Angew. Chem. Int. Ed. **8**, 157–166 (1969)
34. Mulloy, B., Forster, M.J.: Conformation and dynamics of heparin and heparan sulfate. Glycobiology **10**, 1147–1156 (2000)
35. Imberty, A., Chanzy, H., Perez, S., Buleon, A., Tran, V.: The double-helical nature of the crystalline part of A-starch. J. Mol. Biol. **201**, 365–378 (1988)
36. van Eijck, B.P., Mooij, W.T.M., Kroon, J.: Crystal structure prediction for six monosaccharides revisited. J. Phys. Chem. B **105**, 10573–10578 (2001)
37. Appell, M., Strati, G., Willett, J.L., Momany, F.A.: B3LYP/6-311++G** study of alpha- and beta-D-glucopyranose and 1,5-anhydro-D-glucitol: 4C1 and 1C4 chairs, 3, OB and B3,0 boats, and skew-boat conformations. Carbohyd. Res. **339**, 537–551 (2004)
38. Momany, F.A., Appell, M., Willett, J.L., Schnupf, U., Bosma, W.B.: DFT study of alpha- and beta-D-galactopyranose at the B3LYP/6-311++G** level of theory. Carbohyd. Res. **341**, 525–537 (2006)
39. Appell, M., Willett, J.L., Momany, F.A.: DFT study of alpha- and beta-D-mannopyranose at the B3LYP/6-311++G** level. Carbohyd. Res. **340**, 459–468 (2005)
40. Talbot, F.O., Simons, J.P.: Sugars in the gas phase: the spectroscopy and structure of jet-cooled phenyl beta-D-glucopyranoside. Phys. Chem. Chem. Phys. **4**, 3562–3565 (2002)
41. Jockusch, R.A., Talbot, F.O., Simons, J.P.: Sugars in the gas phase - Part 2: the spectroscopy and structure of jet-cooled phenyl beta-D-galactopyranoside. Phys. Chem. Chem. Phys. **5**, 1502–1507 (2003)
42. Mayorkas, N., Rudic, S., Cocinero, E.J., Davis, B.G., Simons, J.P.: Carbohydrate hydration: heavy water complexes of alpha and beta anomers of glucose, galactose, fucose, and xylose. Phys. Chem. Chem. Phys. **13**, 18671–18678 (2011)
43. Brown, D.J., Stefan, S.E., Berden, G., Steill, J.D., Oomens, J., Eyler, J.R., Bendiak, B.: Direct evidence for the ring opening of monosaccharide anions in the gas phase: photodissociation of aldohexoses and aldohexoses derived from disaccharides using variable-wavelength infrared irradiation in the carbonyl stretch region. Carbohyd. Res. **346**, 2469–2481 (2011)
44. Schindler, B., Joshi, J., Allouche, A.R., Simon, D., Chambert, S., Brites, V., Gaigeot, M., Compagnon, I.: Distinguishing isobaric phosphated and sulfated carbohydrates by coupling of mass spectrometry with gas phase vibrational spectroscopy. Phys. Chem. Chem. Phys. **16**, 22131–22138 (2014)
45. Simons, J.P., Jockusch, R.A., Carcabal, P., Hunig, I., Kroemer, R.T., Macleod, N.A., Snoek, L.C.: Sugars in the gas phase. Spectroscopy, conformation, hydration, cooperativity, and selectivity. Int. Rev. Phys. Chem. **24**, 489–531 (2005)
46. Mino, W.K., Gulyuz, K., Wang, D., Stedwell, C.N., Polfer, N.C.: Gas-phase structure and dissociation chemistry of protonated tryptophan elucidated by infrared multiple-photon dissociation spectroscopy. J. Phys. Chem. Lett. **2**, 299–304 (2011)
47. Gulyuz, K., Stedwell, C.N., Wang, D., Polfer, N.C.: Hybrid quadrupole mass filter/quadrupole ion trap/time-of-flight-mass spectrometer for infrared multiple photon dissociation spectroscopy of mass-selected ions. Rev. Sci. Instrum. **82**, (2011)
48. Allouche, A.R.: Gabedit—a graphical user interface for computational chemistry softwares. J. Comput. Chem. **32**, 174–182 (2011)
49. Frisch, M.J., Trucks, G.W., Schlegel, H.B., Scuseria, G.E., Robb, M.A., Cheeseman, J.R., Scalmani, G., Barone, V., Mennucci, B., Petersson, G.A., Nakatsuji, H., Caricato, M., Li, X., Hratchian, H.P., Izmaylov, A.F., Bloino, J., Zheng, G., Sonnenberg, J.L., Hada, M., Ehara, M., Toyota, K., Fukuda, R., Hasegawa, J., Ishida, M., Nakajima, T., Honda, Y., Kitao, O., Nakai, H., Vreven, T., Montgomery, J., J. A.; Peralta, J. E., Ogliaro, F., Bearpark, M., Heyd, J.J., Brothers, E., Kudin, K.N., Staroverov, V.N., Kobayashi, R., Normand, J., Raghavachari, K., Rendell, A., Burant, J. C., Iyengar, S.S., Tomasi, J., Cossi, M., Rega, N., Millam, N.J., Klene, M., Knox, J.E., Cross, J.B., Bakken, V., Adamo, C., Jaramillo, J., Gomperts, R., Stratmann, R.E., Yazyev, O., Austin, A.J., Cammi, R., Pomelli, C., Ochterski, J.W., Martin, R.L., Morokuma, K., Zakrzewski, V.G., Voth, G.A., Salvador, P., Dannenberg, J.J., Dapprich, S., Daniels, A.D., Farkas, O., Foresman, J.B., Ortiz, J.V., Cioslowski, J., Fox, D.J.: Gaussian 09. Gaussian, Inc.: Wallingford, CT (2009)
50. Jebber, K.A., Zhang, K., Cassady, C.J., ChungPhillips, A.: Ab initio and experimental studies on the protonation of glucose in the gas phase. J. Am. Chem. Soc. **118**, 10515–10524 (1996)
51. Ma, B.Y., Schaefer, H.F., Allinger, N.L.: Theoretical studies of the potential energy surfaces and compositions of the D-aldo- and D-ketohexoses. J. Am. Chem. Soc. **120**, 3411–3422 (1998)
52. Sattelle, B.M., Almond, A.: Is N-acetyl-d-glucosamine a rigid $^4C_1$ chair? Glycobiology **21**, 1651–1662 (2011)
53. Heaton, A.L., Armentrout, P.B.: Experimental and theoretical studies of sodium cation interactions with D-arabinose, xylose, glucose, and galactose. J. Phys. Chem. A **112**, 10156–10167 (2008)
54. Nishida, Y., Ohrui, H., Meguro, H.: ^{1}H-NMR Studies of (6r)- and (6s)-deuterated D-hexoses: assignment of the preferred rotamers about C5–C6 bond of D-glucose and D-galactose derivatives in solutions. Tetrahedron Lett. **25**, 1575–1578 (1984)
55. Tvaroska, I., Taravel, F.R., Utille, J.P., Carver, J.P.: Quantum mechanical and NMR spectroscopy studies on the conformations of the hydroxymethyl and methoxymethyl groups in aldohexosides. Carbohydr. Res. **337**, 353–367 (2002)
56. Kouwijzer, M.L.C.E., van Eijck, B.P., Kooijman, H., Kroon, J.: Extension of the GROMOS force field for carbohydrates, resulting in improvement of the crystal structure determination of alpha-D-galactose. Acta Crystallogr. B **330**, 393–393 (1995)
57. Thibodeaux, D.P., Johnson, G.P., Stevens, E.D., French, A.D.: Crystal structure of penta-O-acetyl-beta-D-galactopyranose with modeling of the conformation of the acetate groups. Carbohydr. Res. **337**, 2301–2310 (2002)
58. Longchambon, F., Ohannessian, J., Avenel, D., Neuman, A.: Crystal-structure of beta-D-galactose and alpha-L-fucose. Acta Crystallogr. B **31**, 2623–2627 (1975)
59. Shallenberger, R.S.: Advanced sugar chemistry. AVI Publishing, Westport, CT (1982)
60. Longchambon, F., Gillierpandraud, H., Becker, P.: Crystal-structure of alpha-DL-fucopyranose. Acta Crystallogr. B **33**, 2094–2097 (1977)
61. Kovacs, A., Nyerges, B., Izvekov, V.: Vibrational analysis of N-acetyl-alpha-D-glucosamine and beta-D-glucuronic acid. J. Phys. Chem. B **112**, 5728–5735 (2008)
62. Pohl, A., Dessmann, N., Dutzi, K., Hubers, H.W.: Identification of unknown substances by terahertz spectroscopy and multivariate data analysis. J. Infrared. Milli. Terahz. Waves. **37**, 175–188 (2016)